# Sequential biological and photocatalysis based treatments for shipboard slop purification: a pilot plant investigation

F. Parrino[b], S.F. Corsino[a]*, M. Bellardita[b], V. Loddo[b], L. Palmisano[b], M. Torregrossa[a], G. Viviani[a]

[a] Dipartimento di Ingegneria Civile, Ambientale, Aerospaziale, dei Materiali (DICAM), Università degli Studi di Palermo, Viale delle Scienze Ed. 8, 90128 Palermo, Italy.

[b] Dipartimento di Energia, Ingegneria dell'Informazione e Modelli Matematici (DEIM), Università degli Studi di Palermo, Viale delle Scienze Ed. 6, 90128 Palermo, Italy.

*Corresponding author: santofabio.corsino@unipa.it

**Abstract**

This study investigated the treatment of a shipboard slop containing commercial gasoline in a pilot plant scale consisting of a membrane biological reactor (MBR) and photocatalytic reactor (PCR) acting in series.

The MBR contributed for approximately 70% to the overall slop purification. More precisely, the biological process was able to remove approximately 40%, on average, of the organic pollution in the slop. Nevertheless, the membrane was capable to retain a large amount of organic molecules within the system, amounting for a further 30% of the influent total organic content removal. However, this affected the membrane fouling, thus resulting in the increase of the pore blocking mechanism that accounted for approximately 20% to the total resistance to filtration ($2.85 \cdot 10^{13}$ $m^{-1}$), even if a significant restoration of the original membrane permeability was obtained after chemical cleanings. On the other hand, the biological treatment produced a clear solution for the photocatalytic system, thereby optimizing the light penetration and generation of highly oxidizing active oxygen species that enabled the degradation of bio-recalcitrant compounds. Indeed, low total organic carbon (TOC) values (<10 mg $L^{-1}$) were achieved in the output of the photocatalytic reactor by means of only 60 Einstein (E) of cumulative impinging energy after the addition of $K_2S_2O_8$. Overall, coupling the two processes enabled very high TOC removal (ca. 95%).

**Keywords:** Integrated AOPs; photocatalysis; MBR; saline wastewater; slop.

## 1. Introduction

Shipboard slops and bilge waters represent relevant sources of marine pollution and a real threat for the human and environment health. The complexity of these effluents, in terms of variable composition and concentration of the pollutants, makes the treatment of these wastes an issue of considerable technical and scientific interest (Marpol 73/78, 2006).

Due to their simple applicability, physic-chemical processes are the most commonly techniques used to face this issue. However, the oils separation by gravity is often a very high-time demanding process and the majority of the pollutant compounds are not chemically degraded but only separated and transferred to other phases. Therefore, further treatments must be performed downstream of these processes. Furthermore, the removal efficiency of the main pollutants does not fit the targets imposed by the current legislation. Therefore, physic-chemical processes could be considered only preliminary treatments, to be implemented upstream to more efficient purification processes.

In recent years, the scientific community has put forward many efforts toward the use of biological treatments instead of the chemical-based ones. Indeed, biological processes can relieve most of the carbon content of wastewater with minimal energy requirements and without generating secondary pollution. Among the biological processes, membrane bioreactors (MBRs) technology allows to obtain very high-quality effluents and at the same time is featured by small footprint and low excess sludge production (de Oliveira et al., 2018; Salerno et al., 2017). Recently, MBRs have been successfully applied for the treatment of slops (Campo et al., 2017b; Capodici et al., 2017). However, the biological removal efficiency of the organic pollution obtained under high salinity conditions does not always fit the standards imposed by the current legislation. Indeed, biodegradation of petroleum hydrocarbons is a complex task due to their complex chemical nature and their xenobiotic behaviour. Consequently, significant amounts of recalcitrant and toxic compounds, even at very low concentrations, pass through the biological process unaltered.

The use of advanced oxidation processes (AOPs) may be a promising solution for this problem. Among the AOPs, heterogeneous photocatalysis has been successfully used to oxidize many organic pollutants present in aqueous systems (Augugliaro et al., 1997, 1994). Titanium dioxide ($TiO_2$) is the most studied and used semiconductor to this aim. Indeed, it is inexpensive, photo-chemically stable, non-hazardous and very versatile. On the other hand, photocatalytic treatments of highly saline effluents suffer of very slow purification efficiency because of the presence of chloride ions and the low oxygen concentration in solution deriving from the high ionic strength of the reacting medium. For this reason, photocatalysis should be applied to clear solutions with relatively low content of organic compounds. Indeed, the presence of solids or very high pollutants concentration strongly limits the light penetration through the reacting mixture, thus dramatically affecting the efficiency of the process.

Bearing in mind the above-mentioned issues, coupling a biological treatment with a photocatalytic one could represent a promising alternative for slops and bilge water treatment. In fact, the biological process could simultaneously reduce the initial organic content and the turbidity of the wastewater to suitable levels for the photocatalytic treatment, which, on the other hand, would ensure the mineralization of organic species that are recalcitrant to biological degradation. In this way, the integration of different technologies could allow overcoming the drawbacks of these methods used separately. To the best of our knowledge, the present study is the first report on a photocatalysis $TiO_2$ based process with upstream biological treatments for saline wastewater purification at a pilot plant scale.

In this paper, we propose a photocatalytic treatment downstream to the biological one in order to optimize the photocatalytic conditions in terms of light distribution and efficiency. The contributions of the single biological, membrane, and photocatalytic systems have been investigated in terms of TOC (total organic carbon) removal.

## 2. Materials and methods

### *2.1 Simulated slop composition*

The artificial wastewater was prepared based on characterizations carried out on real slops. More precisely, the results obtained from the TOC analysis of different real samples or slops (S1-S5) collected from coastal storage of petroleum products are reported in Table 1 (Cataldo et al., 2016).

**Tab. 1.** TOC values of five real slop samples. Standard error: ±0.05 $mg \cdot L^{-1}$

| Real slop sample | TOC [$mg \cdot L^{-1}$] |
|---|---|
| S1 | 74.70 |
| S2 | 86.20 |
| S3 | 85.00 |
| S4 | 101.00 |
| S5 | 79.55 |

The results revealed moderate variability for organic contaminant concentrations, which mainly depended on the pre-treatment processes used (coagulation/flocculation or physical oil separation). The determined $Cl^-$ ion content was similar for all of the samples and corresponded to the typical concentration in seawater (ca. 0.56 M).

The pilot plant was fed with a synthetic wastewater simulating a shipboard slop after a pre-treatment by means of a de-oiling process. Moreover, to prevent any limitation to the biological process, rapidly biodegradable organic matter, nitrogen and phosphorous, in the form of $CH_3COONa$, $NH_4Cl$, and $K_2HPO_4$, respectively, were added to obtain a C:N:P ratio equal to approximately 100:5:1.

The composition and the main features of the synthetic slop are reported in Table 2:

**Tab. 2:** Composition and average characteristics of the synthetic slop.

| Synthetic slop composition (in 500 L of tap water) | | |
|---|---|---|
| Compound | Unit | Value |
| Diesel | mL | 25 |
| SDBS | g | 100 |
| Sodium Chloride | kg | 10 |
| Ammonium Chloride | g | 60 |
| Potassium bi-phosphate | g | 16 |
| **Synthetic slop features** | | |
| Parameter | Unit | Value |
| TPH | mg $L^{-1}$ | 31±0.5 |
| TOC | mg $L^{-1}$ | 224±13.2 |
| TN | mg $L^{-1}$ | 16.4±0.7 |
| TP | mg $L^{-1}$ | 8.6±0.4 |
| Electrical conductivity | mS $cm^{-1}$ | 35 |

Legend: SDBS= Sodium Dodecyl Benzene Sulfonate; TPH= Total Petroleum Hydrocarbon; TOC= Total Organic Carbon; TN: Total Nitrogen; TP: Total Phosphorous

*2.2 Pilot plant layout*

The pilot plant installation consisted of a combined system including an MBR followed by a photocatalytic reactor (PCR). The pilot plant layout is depicted in Figure 1.

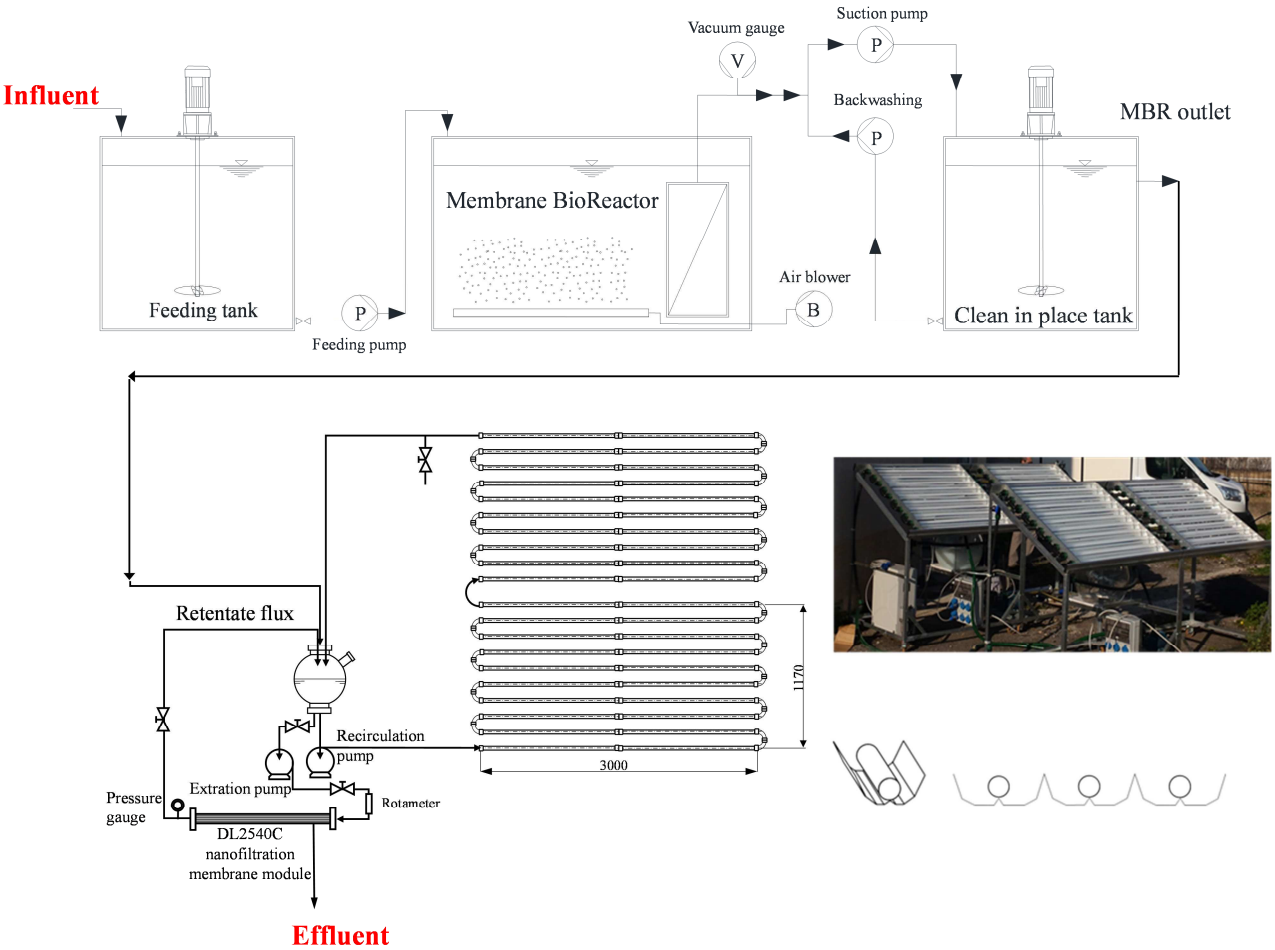

**Fig. 1:** Schematic layout of the MBR-PCR pilot plant installation. In the inset a picture of the photocatalytic reactor and a scheme of the reflectors.

The MBR pilot plant consisted of a feeding tank (V = 500 L) equipped with a mechanical stirrer in which the synthetic slop was stored. From this tank, the slop was pumped to the biological reactor (190 L) with a flow equal to 4 L $h^{-1}$. The biological reactor was equipped with an ultrafiltration (UF) hollow fibers membrane module (*Koch Puron*®) (specific area equal to 0.47 $m^2$ and nominal porosity of 0.03 μm), according to the submerged configuration (Judd, 2006), which provided the permeate extraction. The MBR effluent permeate was stored into a "clean in place" (CIP) tank that was used as compensation volume for both the membrane backwashing and the photocatalytic reactor feeding. The photocatalytic reactor has been designed to treat the same flow of the MBR (96 L $d^{-1}$) but in batch mode. It was a non-continuous total recirculation reactor consisting of four modules (irradiated surface: 7.5 $m^2$) in aluminium with 10 Pyrex tubes (diameter 32 mm and length 1500 mm) each connected with polymeric flanges. In order to optimize the irradiation of the photocatalytic suspension, aluminium parabolic collectors have been positioned beneath the tubes. From the CIP tank, the MBR permeate was sent by gravity into a chamber by opening a timed valve. From the loading chamber, a centrifuge pump provided the liquid circulation within the photocatalytic modules. The system was equipped with a nanofiltration membrane (DL2540C type) to separate the photocatalyst from the effluent PCR permeate. A pump ensured the recirculation of the suspension and a high prevalence pump allowed the fluid to be filtered through the membrane. The nanofiltration retentate, containing the residual photocatalyst, was returned to the loading chamber.

*2.3 MBR operating conditions*

To prevent the membrane fouling, the flux across the membrane was maintained close to 10 L $m^{-2}$ $h^{-1}$, according to the manufacturer suggestions. The membrane was periodically backwashed (1

157 minute every 5 minutes) by pumping a fraction of the permeate back through the membrane
158 module. The net permeate flow was equal to 4 $L^{-1}h^{-1}$, thereby resulting in a daily flow of 96 L $d^{-1}$.
159 Accordingly, the hydraulic retention time (HRT) of the MBR pilot plant resulted of approximately
160 48 h. When the transmembrane pressure (TMP) was higher than 0.6-0.7 bar (value suggested by the
161 membrane manufacturer), the filtration was stopped and the membrane permeability was restored
162 by means of physical (hydraulic/sponge scrubbing), and/or chemical washings (at the end of the
163 experiment). The MBR pilot plant was started-up with activated sludge characterized by a mixed
164 liquor suspended solids (MLSS) concentration of 2 g $L^{-1}$ previously acclimated at 20 g $L^{-1}$ NaCl of
165 salinity. The acclimation phase consisted of a period (3 months) during which the MBR was fed
166 first only with a synthetic saline medium without hydrocarbons. During this phase, the influent
167 wastewater was characterized by an increasing salt concentration from 0 gNaCl $L^{-1}$ to 20 gNaCl $L^{-1}$.
168 After the biomass was acclimated to salinity, hydrocarbons were added to the synthetic medium at a
169 concentration of 20 mgTPH $L^{-1}$ in the form of diesel fuel. The fuel was composed by a
170 hydrocarbons' mixture ranging from C10 to C30. The hydrocarbon concentration and the maximum
171 threshold of salinity were chosen to simulate a shipboard slop already subjected to physical-
172 chemical pre-treatment.
173 The sludge retention time (SRT) was not controlled and no dedicated wasting operations of sludge
174 were performed, excepting the samples withdrawn to perform chemical-physical analyses.
175 Therefore, it can be assumed that the pilot plant was operated with a complete sludge retention
176 strategy.
177
178 *2.4 Photocatalysis operating conditions*
179 The $TiO_2$ photocatalysts used for the present investigation were labelled as P25 and P25son. P25
180 sample, purchased from Evonik, consisted of a mixture of anatase (80%) and rutile (20%) and were
181 characterized by a specific surface area of ca. 50 $m^2$ $g^{-1}$. P25son has been obtained from P25
182 according to a procedure reported elsewhere (Bellardita et al., 2017) and hereby briefly described.

A slurry containing 10 g of P25 dispersed in 150 mL of demineralised water was sonicated for 2 h in an ultrasonic bath operating at 40 kHz equipped with a cooling system that maintained the temperature at ca. 5 °C. Finally, the powder was filtered and dried at 80 °C for 24 h. Potassium peroxydisulfate ($K_2S_2O_8$) (Sigma Aldrich, p.a.) was used as received without further purification.

If not otherwise specified, the photocatalytic runs were performed daily (ca. 8 h per run) on 96 L solution downstream to the biological treatment at ambient temperature and pressure in the presence of air. The catalyst concentration used for each run was 0.2 g $L^{-1}$. This amount of catalyst ensured the optimum photon absorption. Selected runs were carried out in the presence of 2 g $L^{-1}$ potassium peroxydisulfate ($K_2S_2O_8$). This value was approximately one third of the amount of $K_2S_2O_8$ required for the complete mineralization of the substrate based on the mean oxidation state of the carbon atom content. Irradiation was both artificial and solar. More precisely, artificial irradiation (UV emission: 21 W $m^{-2}$) was performed by means of two modules in aluminium containing 10 fluorescent tubes UVA each, with an irradiance power of 80 W provided with reflectors and positioned in line with the Pyrex tubes where the suspension circulated. Figure S1 shows some pictures of the artificial irradiation.

**Figure S1:** Artificial irradiating system.

Photocatalytic experiments have been carried out in Sicily (Palermo, 38°7'N/13°22'E) under natural sunlight during sunny days. During natural sunlight irradiation, the panels faced south. The tilt angle of the panels with respect to the ground (ca. 32°) was calculated by taking into account the mean height of the sun (highest during the summer solstice and lowest during winter solstice) at the latitude of the plant.

In order to compare the results and ensure reproducibility, the photoactivity results obtained under different irradiation conditions have been plotted versus the cumulative photonic energy incident on the reactor, $E_{hv}$, rather than versus irradiation time (Malato Rodriguez et al., 1996).

This quantity is given by the equation 1:

$$E_{hv} = \int_0^t \Phi_P \, dt \qquad (1)$$

where $\Phi_P$ is the photon flow [Einstein/s] and t the irradiation time. The values of $\Phi_P$ were calculated from the irradiance data, by using the following relationship:

$$\Phi_P = UV_G \cdot S \qquad (2)$$

where S is the geometrical irradiated surface (7.5 $m^2$) and $UV_G$ the irradiance measured during the reaction time expressed as $W/m^2$. The $UV_G$ dimensions have been transformed in [Einstein] by using the Planck's equation ($E=hc/\lambda$).

*2.5 Analytical methods*

Total organic carbon (TOC) was used as the indicator to assess the system performances. The TOC concentration was measured at the inlet and the outlet of the MBR system, as well as in the mixed liquor supernatant, in order to single out the removal efficiency of the biological process and filtration provided by the membrane. In this way, two different removal efficiencies were calculated: the biological removal efficiency and the total removal efficiency of the MBR compartment. The biological removal efficiency was calculated as the difference between the TOC value in the influent and the TOC measured in the supernatant of mixed liquor samples (after

centrifugation at 5000 rpm for 5 minutes) withdrawn from the MBR tank. The total TOC removal efficiency of the MBR (including also the retention effect of the membrane filtration) was assessed as the difference between the TOC in the influent and the TOC measured in the MBR permeate samples.

In the PCR, the TOC values were measured before the addition of the catalyst and before starting the irradiation, in order to obtain the substrate concentration after the achievement of adsorption-desorption equilibrium. Consequently, the extent of the substrate adsorption on the catalyst surface under dark conditions was determined. During the reactions, samples withdrawn at fixed times were immediately filtered through 0.45 mm membranes (HA, Millipore) before TOC analyses. The radiation intensity impinging on the suspension was measured by a radiometer Delta Ohm DO9721 with an UV-A probe.

All the TOC measurements were performed by means of thermo-catalytic oxidation with a high-temperature TOC-VCSH analyzer.

The measurement of total suspended solids (TSS) and of volatile suspended solids (VSS) concentration was performed according to the standard methods (Apha, 2005).

Extracellular polymeric substances (EPSs) extraction was carried out in accordance with the Heating Method described in literature (Le-Clech et al., 2006). Therefore, for both SMPs and EPS, the polysaccharides and protein concentrations were determined according to the phenol-sulphuric acid method with glucose as the standard (DuBois et al., 1956) and by the Folin method with bovine serum albumin as the standard (Lowry et al., 1951), respectively. The size and morphology of the activated sludge flocs were examined by means of a high-speed image analyses sensor (Sympatec Qicpic) that provided the particle size distribution and the granulometric curve.

The membrane fouling analysis was carried out by measuring the total resistance to filtration ($R_T$) according to the following equation 3:

$$R_T = \frac{TMP}{\mu \cdot J} \qquad (3)$$

where $R_T$ is the total fouling resistance ($10^{12}$ $m^{-1}$) calculated by the general form of Darcy's Law, TMP is the transmembrane pressure (Pa), μ the permeate viscosity (Pa·s), and J the permeation flux (m $s^{-1}$). The resistance-in-series (RIS) model was applied with the aim to investigate the specific deposition mechanisms (Di Bella et al., 2018).

## 3. Results and Discussion

### *3.1 Biomass growth and activated sludge characteristics*

Figure 2a depicts the trends of the mixed liquor TSS concentration and the VSS/TSS ratio during the experiment.

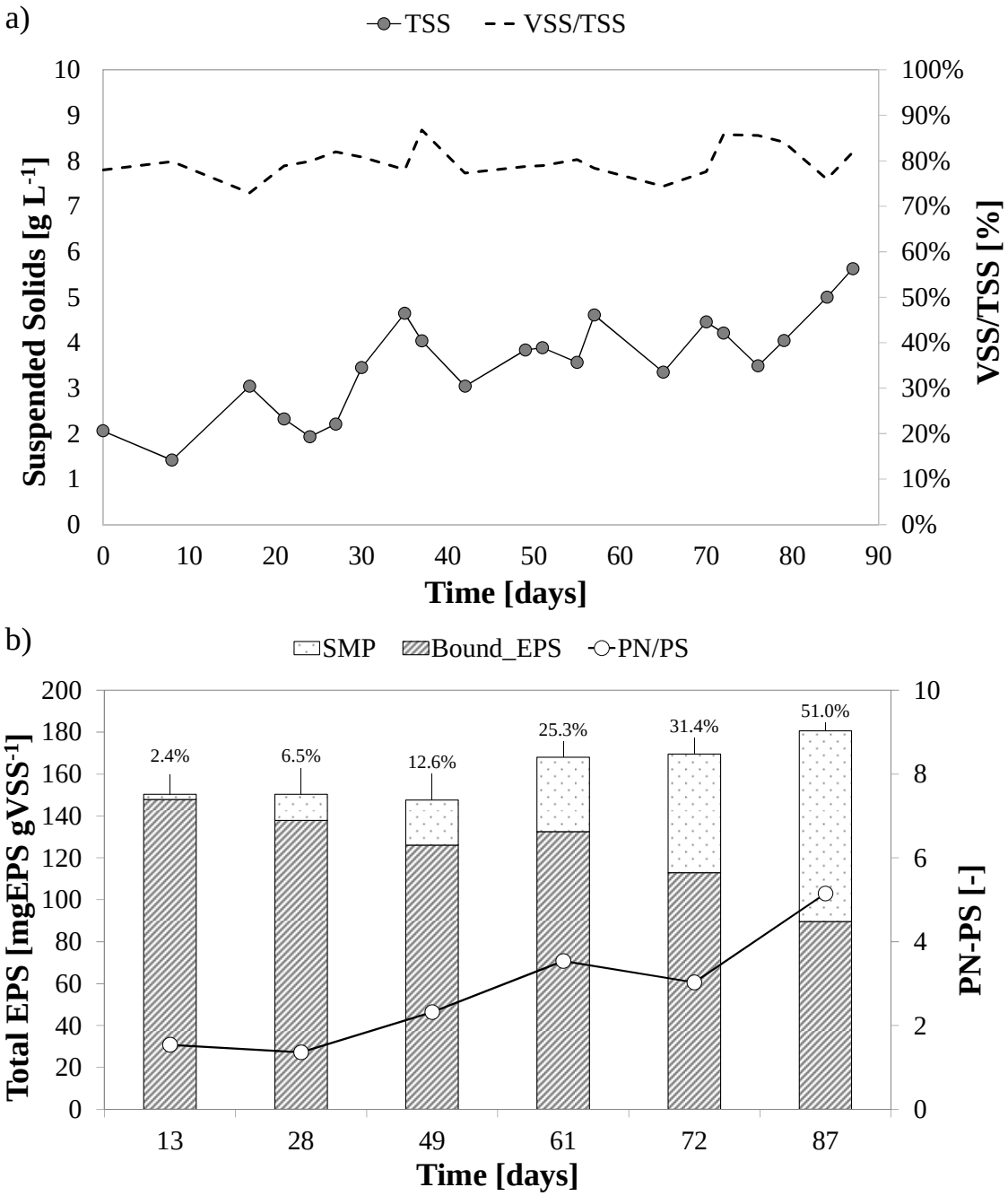


Legend: SMP= Soluble Microbial Products; EPS: Extracellular Polymeric Substances; PN= Proteins; PS= Polysaccharides.

**Fig. 2:** Trends of the total suspended solid concentration (TSS) and volatile suspended solid/total suspended solid (VSS/TSS) ratio in the mixed liquor during the experiments (a); amount and composition of the EPS (b).

As aforementioned, the MBR was seeded with a MLSS concentration of 2 g TSS $L^{-1}$. During the entire experiment, an increasing trend of the TSS concentration was observed. Indeed, the suspended biomass of the MBR plant constantly increased reaching a value of approximately 5.5 g TSS $L^{-1}$ at the end of observed period. This result indicated a good biomass activity although the stress-effect exerted by the hydrocarbons and the saline environment. Accordingly, the VSS/TSS ratio was almost constant at a value of approximately 0.80 during the entire experiment, thereby indicating that no accumulation of inert material within the activated sludge flocs occurred.

The trends of the EPS amount and composition are shown in Figure 2b. The specific total EPS amount of the activated sludge showed a slightly increasing trend from approximately 150 mg EPS g $VSS^{-1}$ to 180 mg EPS g $VSS^{-1}$ during the experiment. Although the average EPS amount was constant, the EPS structure and composition significantly changed. Indeed, the bound EPS content decreased, while at the same time that of the SMP increased. More precisely, the SMP fraction of the total EPS increased from approximately 2% (value of the inoculum) to 50% at the end of the observed period. This result clearly indicated that hydrolysis of the bound EPS occurred during the experiment. This led to the increase of the soluble EPS fraction (>200%), whose accumulation within the bulk was favoured by the membrane retention ability. This was demonstrated by the EPS measures performed in the permeate that revealed that neither proteins nor carbohydrate were detected. One possible explanation to this result is that the low biodegradability of the slop led microorganisms to use the EPS as carbon source for their metabolism (Zhang and Bishop, 2003). Similarly, the EPS composition changed during the experiment. More precisely, the protein (PN) to polysaccharides (PS) ratio in the bound EPS increased from approximately 1.5 to 5.15 during the entire experiment. This result was in good agreement with other studies (Corsino et al., 2017; Di Bella et al., 2015; Mannina et al., 2016), in which the authors observed that the increase of the proteinaceous EPS was likely due to a stress effect exerted by hydrocarbons. The bound EPS caused by the loss in the stability of the activated sludge flocs. Indeed, the activated sludge flocs morphology gradually changed into small and irregular flocs with an average size constantly

290 decreasing from 90 µm (seed sludge) to 50 µm at the end of the experiment. Although
291 deflocculation generally occur in MBR system, in this case this phenomenon was likely worsened
292 by the EPS destructuration.
293
294 *3.2 Organic removal in MBR*
295 Figure 3 shows the TOC removal observed in the MBR system. More precisely, the Figure 3a
296 depicts the trend of the TOC in the influent and in the supernatant of the MBR tank, as well as in
297 the permeate (Fig. 3a), whereas Figure 3b shows the biological and the physical contributions to the
298 overall TOC removal efficiency during the experiment.

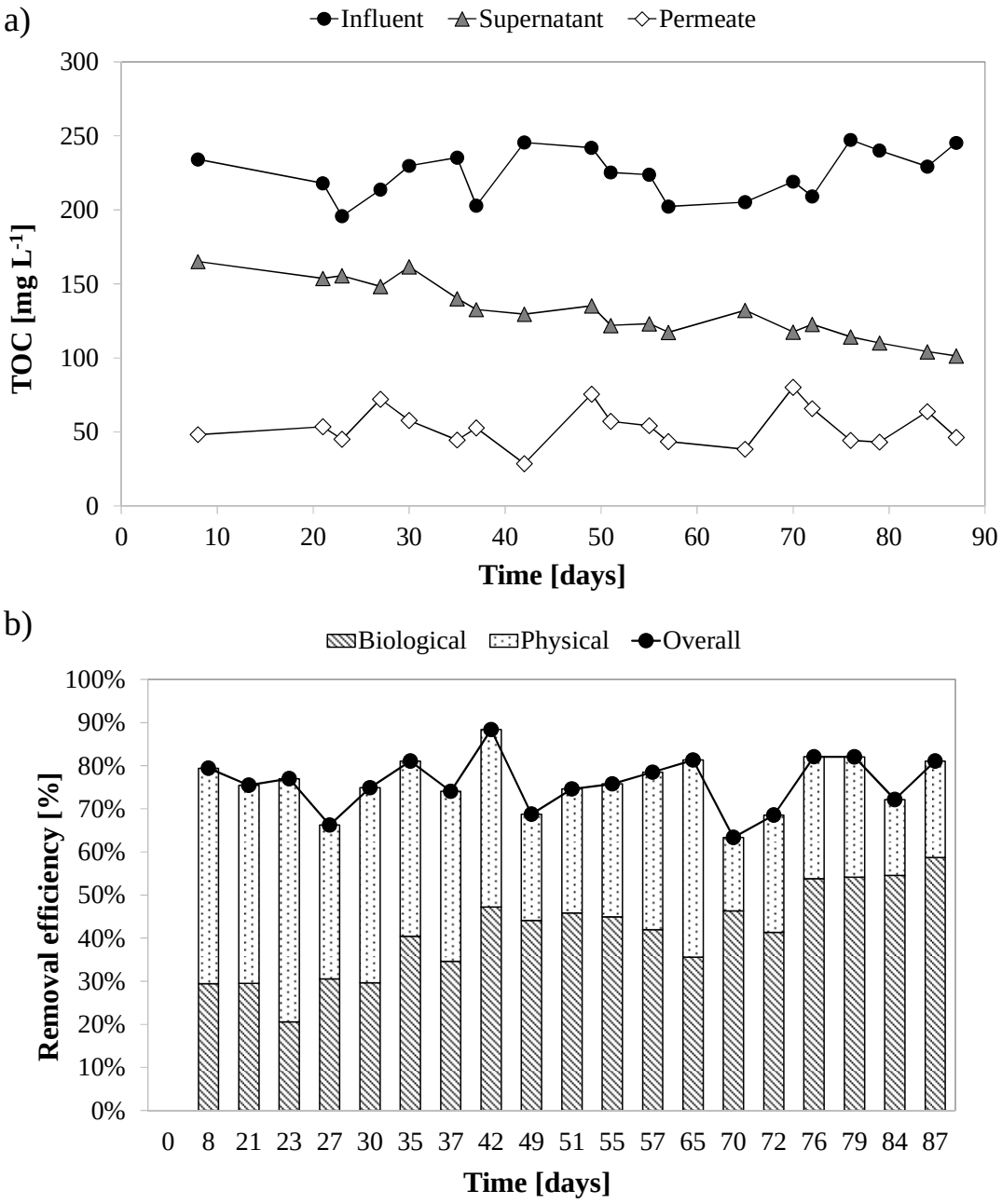


**Fig. 3:** TOC concentration in the inlet, outlet and supernatant of the MBR system (a); biological, physical and overall TOC removal efficiencies throughout the experiment (b).

In terms of TOC removal, the MBR enabled a good removal efficiency throughout the experiment. Indeed, the TOC removal was close to 80% on average, confirming the robustness of the MBR system for the treatment of recalcitrant wastewater.

306 The biological contribution (average value) was close to 40%, indicating that the biological process
307 was not able to ensure a complete degradation of the organic pollution in the slop. The TOC in the
308 supernatant ranged between 110 mg $L^{-1}$ and 160 mg $L^{-1}$, showing an overall decreasing trend during
309 entire experiment. This result was in good agreement with the increase of the biomass concentration
310 previously discussed. Therefore, the increase of the biomass concentration contributed to the
311 improvement of the biological process. Based on the results, it is possible to speculate that as the
312 specific biodegradation rate of hydrocarbons is limited by the structural complexity of the
313 molecules, to achieve satisfactory biological removal efficiencies it would be advisable to operate
314 with higher biomass concentrations. Nonetheless, although the TSS concentration constantly
315 increased during the entire experiment, the biological TOC removal efficiency reached a stable
316 value close to 55% on the 76$^{th}$ day and this value was almost constant until the end of the observed
317 period. Moreover, the obtained results in terms of TOC removal were comparable with those
318 obtained in previous studies carried out under similar operating conditions and for a longer period
319 (Di Bella et al., 2015; Viero et al., 2008). Therefore, it can be speculated that the maximum
320 biodegradation capacity by microorganisms was already achieved. In other words, it is likely that
321 the residual TOC was constituted by not-biodegradable organic substances, therefore, no further
322 improvements in biological performance could be achieved even with a higher biomass
323 concentration.
324 The TOC concentration in the permeate ranged between 30 mg $L^{-1}$ and 70 mg $L^{-1}$, indicating that
325 the physical retention of the membrane significantly contributed to the overall TOC removal.
326 Specifically, the physical contribution of the membrane was close to 35% (average value) of the
327 total TOC removal efficiency. It is possible to speculate that the membrane was able to retain within
328 the reactor all the molecules characterized by a dimension bigger than the membrane pore size (0.03
329 µm), thereby resulting in a further increase of the TOC removal performance. Notably, the
330 membrane retention capacity decreased on days 27$^{th}$, 49$^{th}$, 70$^{th}$ and 84$^{th}$ following physical cleanings
331 of the membrane. After each physical cleaning, the removal efficiency showed an increasing trend

until the following physical cleaning was performed. It is reasonable that the cake deposition at the membrane fibers' surface, allowed increasing the retention capacity of the membrane towards smaller molecules, because the cake acted as a pre-filter, although it caused additional resistances to the filtration.

However, the value of TOC observed in the permeate, close to 50 mg $L^{-1}$ on average, indicated that a large amount of organic molecules passed through the biological process unaltered, thereby suggesting that a not negligible organic pollution was still present in the effluent of the MBR system.

*3.3 Hydraulic performances: membrane-fouling characterization*

Figure 4 depicts the membrane fouling trends in terms of total resistance ($R_T$) (a) and its decomposition (b) evaluated according to equation 2, whereas Figs.4 c1-c4 show the percentage of each resistance fraction respect to the total fouling resistance.

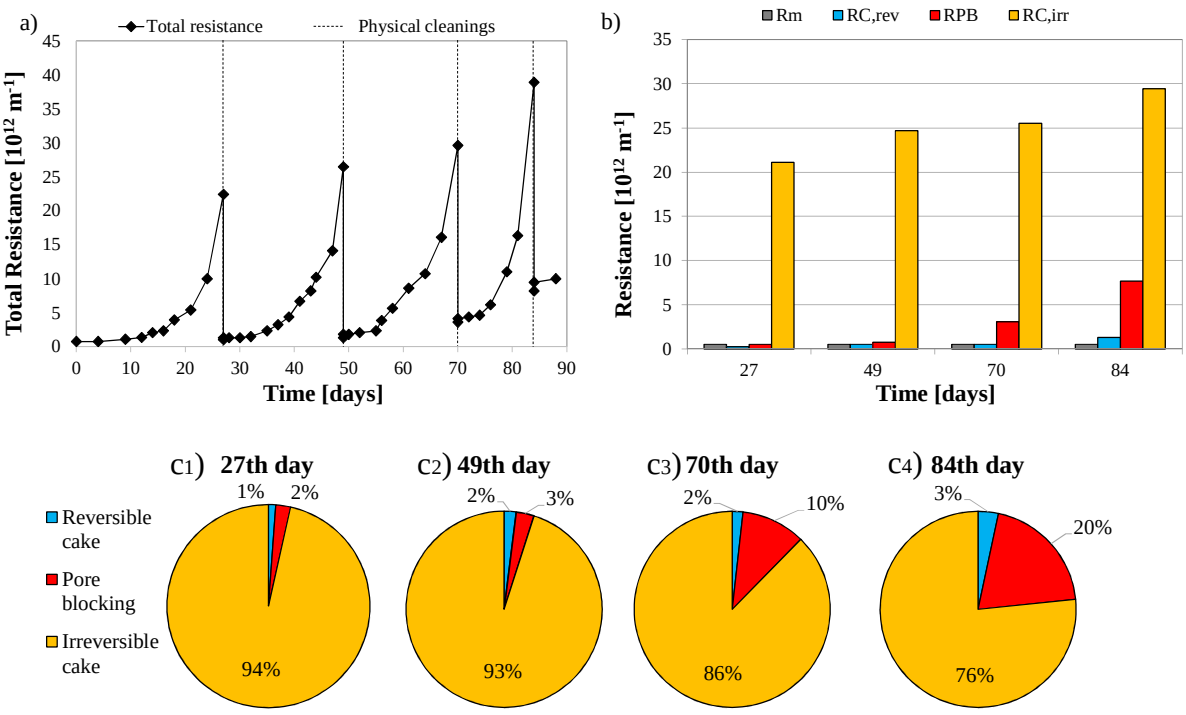

346 **Fig. 4:** Total $R_T$ (a), specific resistances (b), and percentage of each resistance fraction with respect
347 to the total fouling resistance (c1-c4).
348
349 During the experiment, four membrane-cleaning operations were performed. Specifically, physical
350 cleanings were performed on $27^{th}$, $49^{th}$, $70^{th}$ and $84^{th}$ experimental days, when the TMP exceeded
351 0.6 bar, whereas only one chemical cleaning was performed at the end of the experiment. The
352 fouling rate gradually increased during the experiment from approximately 0.80 $m^{-1}$ $d^{-1}$ to 1.85 $m^{-1}$
353 $d^{-1}$, thereby increasing the frequency of the membrane cleaning operations.
354 The irreversible cake due to the superficial cake layer ($R_{C,irr}$) was the highest fraction of the total
355 resistance to filtration. The $R_{C,irr}$ slightly increased from $21 \cdot 10^{12}$ $m^{-1}$ to approximately $30 \cdot 10^{12}$ $m^{-1}$ at
356 the end of the experiment. Beginning in the experiment, the relative contribution of the $R_{C,irr}$ to the
357 $R_T$ was approximately the 94%. However, it gradually decreased to approximately 76% at the end
358 of the observed period (Fig 4c1-c4). A gradual transfer of the fouling mechanism from the "cake
359 layer deposition" directly to the "pore blocking" was observed. Indeed, the irreversible fouling due
360 to pore blocking ($R_{PB}$) significantly increased from approximately the 2% of the $R_T$ to a value of
361 20% on the $84^{th}$ experimental day. Lastly, the contribution of the reversible resistance due to the
362 superficial cake layer ($R_{C,rev}$) was almost constant at the 2-3% of the total resistance, hence it was
363 considered negligible. The increase of the $R_{C,irr}$ was found to be in good agreement with the increase
364 of the proteinaceous EPS and with the decrease of the bound EPS above discussed. Indeed, with
365 regard to the first aspect, the fouling from irreversible cake can be attributable to the increase of
366 proteins, which gave a gelatinous and hydrophobic consistency to the cake that cannot be removed
367 with ordinary backwashes. The increase of the $R_{C,irr}$ following to the bound EPS reduction was in
368 contrast with previous studies in the literature that showed a positive linear correlation between the
369 bound EPS and the fouling due to irreversible cake (Meng et al., 2009). Nevertheless, this result
370 was in line with a previous study carried out in a MBR pilot plant treating saline-oily wastewater, in

371 which a negative correlation between the bound EPS and the fouling from irreversible cake was
372 found (Mannina et al., 2016).
373 The increase of the $R_{PB}$ could be likely related to the activated sludge deflocculation previously
374 discussed. Indeed, previous studies demonstrated that the worsening of the sludge features (i.e.
375 deflocculation and decrease of the bound EPS) caused the decrease of the pre-filter effect exerted
376 by the cake layer (Campo et al., 2017). As previously discussed, the decrease of the bound EPS was
377 followed by the activated sludge deflocculation and the increase of the SMP concentration. A
378 higher concentration of SMP is recognized as an important evidence of the activated sludge
379 deflocculation (Sheng et al., 2008), whose increase could strongly affect the membrane fouling. In
380 this way, due to their low dimension (50-500 kDa), SMP could more easily reach the membrane
381 pores, thus contributing to the increase of the total resistance to filtration due to pore blocking (Lin
382 et al., 2014). Moreover, the increase of the proteinaceous component of the EPS resulted in a further
383 worsening of the fouling. Indeed, proteins are recognized as one of the major foulant agent in MBR
384 due to their hydrophobic interaction with the polymeric structure of the membrane fibers (Campo et
385 al., 2017; Miyoshi et al., 2011). Nonetheless, at the end of the experiment a chemical cleaning of
386 membrane was performed in order to characterize the pore blocking fouling. After the chemical
387 cleaning, more than 98% of the original membrane permeability was recovered, meaning that the
388 irreversible pore blocking (the fouling that cannot be removed even with chemical cleanings) was
389 very low and the membrane service life was not impaired.
390
391 *3.4 Photocatalysis-based process*
392 The mechanism of photocatalytic reactions is well known (Augugliaro, 1994). When light of
393 suitable energy impinges on $TiO_2$ surface, excitation of solid occurs and electrons ($e^-$) and holes ($h^+$)
394 are generated in the conduction and valence bands, respectively. These charges can be trapped by
395 species on the $TiO_2$ surface giving rise to the formation of highly oxidizing species as hydroxyl

radicals ($^{\cdot}OH$) which in turn initiate oxidation reactions. Eqs. 4-9 sum up the above-mentioned mechanism.

$$TiO_2 + h\nu \rightarrow TiO_2\,(e^-, h^+) \quad (4)$$

$$OH^- + h^+ \rightarrow {}^{\cdot}OH \quad (5)$$

$$O_2 + e^- \rightarrow {}^{\cdot}O_2^- \quad (6)$$

$$^{\cdot}O_2^- + H^+ \rightarrow HO_2^{\cdot} \quad (7)$$

$$2HO_2^{\cdot} \rightarrow O_2 + H_2O_2 \quad (8)$$

$$H_2O_2 + {}^{\cdot}O_2^- \rightarrow OH^- + {}^{\cdot}OH + O_2 \quad (9)$$

Preliminary photocatalytic tests have been performed under solar irradiation by treating tap water solutions containing approximately 25 mg $L^{-1}$ of commercial gasoline, in the presence of P25 or P25son. Results are shown in Figure 5.

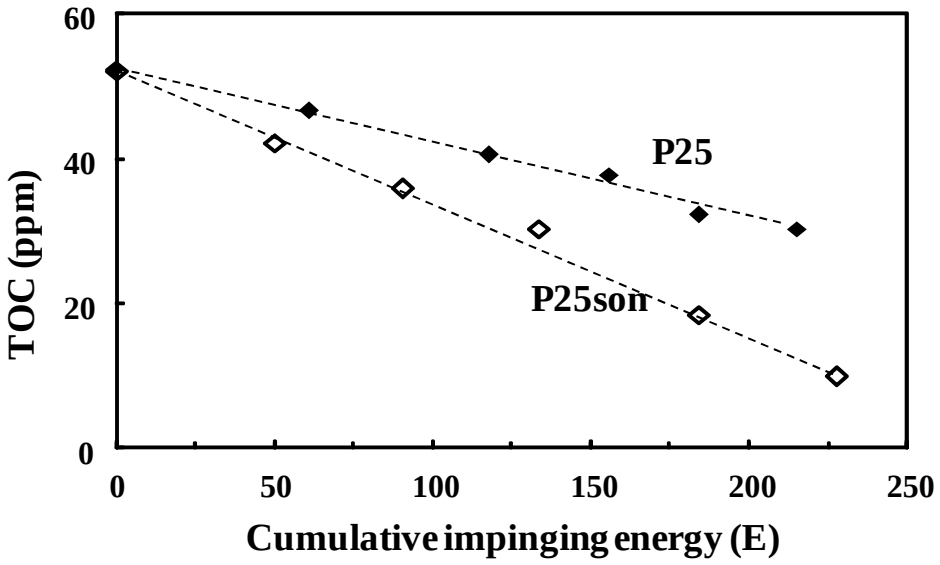


**Fig. 5:** TOC values versus the cumulative energy impinging the photocatalytic suspension (in the absence of NaCl) in the pilot scale reactor under natural sunlight irradiation in the presence of air, 0.2 g $L^{-1}$ of P25 and P25son, at ambient temperature and pressure. Initial TOC concentration: 53 mg $L^{-1}$.

413 Photocatalysis in the absence of NaCl, under solar irradiation, with both P25 and P25son
414 photocatalysts, afforded TOC values, which would allow to safely releasing the effluent in the
415 environment. Notably, P25 resulted less active than P25son under sunlight because the sonication
416 pre-treatment induced lattice defects, which endowed the photocatalyst with visible light absorption
417 as discussed in a previous study (Bellardita et al., 2017). Therefore, while P25 was able to absorb
418 only the UV part of the solar spectrum (which constitutes ca. 4% of the emitted radiation), P25son
419 was activated also by the visible part, thus inducing faster degradation under the given experimental
420 conditions. It is worth mentioning that the organic load used in the present study (commercial
421 gasoline) was constituted by long chain (8-13 C atoms) aliphatic compounds, which were
422 particularly recalcitrant to photocatalytic mineralization. The results above were relevant especially
423 because a large part of the photocatalytic experiments reported in literature consider the degradation
424 of less recalcitrant compounds such as dyes (Khataee and Kasiri, 2010; Šíma and Hasal, 2013).
425 However, when saline water was used instead of tap water, solar irradiation did not induce
426 noticeable degradation of the organic pollutants (results not shown). The ionic strength of the
427 solution reduced the $O_2$ solubility and the chloride ions present in the solution acted as OH radical
428 scavengers (Yang et al., 2005) so that the photocatalytic reaction rate resulted very low. Indeed, a
429 cumulative impinging energy of approximately 80 E (correspondent to 20 hours irradiation)
430 afforded only 3% degradation as shown in Figure 6.

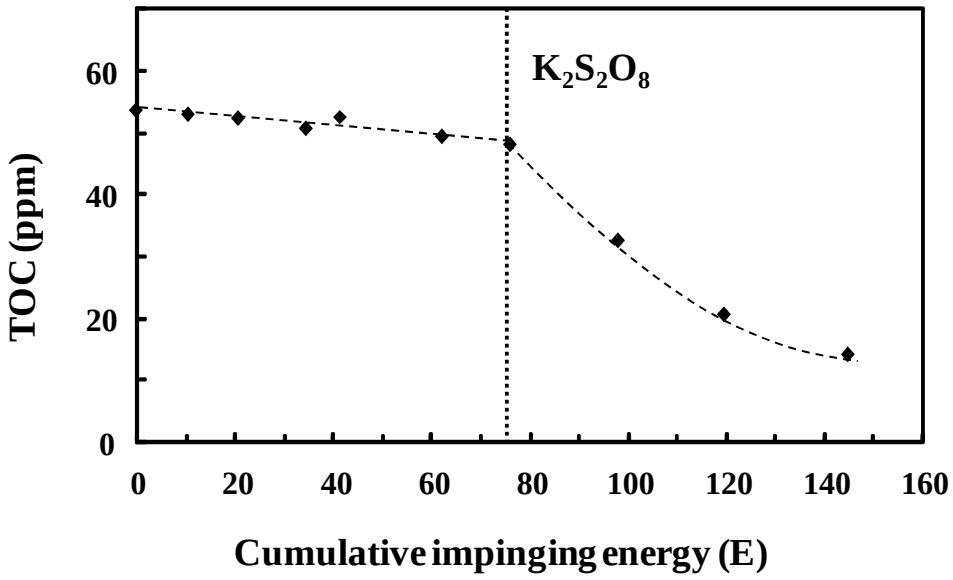


**Fig. 6:** TOC values versus the cumulative energy impinging the solution downstream to the biological treatment in the pilot scale reactor under artificial UV light irradiation in the presence of air, 20 g $L^{-1}$ NaCl, 0.2 g $L^{-1}$ of P25, at ambient temperature and pressure ($87^{th}$ day). After the dotted line $K_2S_2O_8$ (2 g $L^{-1}$) was present in the system. Initial TOC concentration: 54 mg $L^{-1}$.

To enhance the degradation rate, a strong oxidant, as potassium peroxydisulphate ($E_{S_2O_8^{2-}/SO_4^{\bullet-}}$ = 1.1 V) producing harmless sulphate ions, was added. Although it has been reported that potassium peroxydisulfate was effective for degrading some organics through direct chemical oxidation (McCallum et al., 2000), its reaction rate with the recalcitrant compounds hereby considered was very slow in the absence of photocatalysis. On the other hand, peroxydisulfate ions were activated via photochemical, thermal, radiolytic or redox decomposition to generate stronger oxidants such as sulphate radicals ($SO_4^{\bullet-}$, $E^0$ = 2.6 V). In the presence of irradiated $TiO_2$ peroxydisulphate activation occurred through the following equations.

$$S_2O_8^{2-} + e^- \rightarrow SO_4^{2-} + SO_4^{\bullet-} \quad (10)$$

$$SO_4^{\bullet-} + H_2O \rightarrow SO_4^{2-} + {}^{\bullet}OH + H^+ \quad (11)$$

$$SO_4^{\bullet-} + OH^- \rightarrow {}^{\bullet}OH + SO_4^{2-} \quad (12)$$

449

450 The sulfate radicals generated through Eq. 10 and the hydroxyl radicals generated through Eqs. 4, 9,
451 11 and 12 were responsible for the degradation observed in Figure 6. In fact, low TOC values (ca.
452 15 mg·$L^{-1}$) could be reached by means of only 60 E of cumulative impinging energy after the
453 addition of $K_2S_2O_8$.

454

455 *3.4 Performance of the MBR-PCR system*

456 The overall performance of the MBR-PCR during the entire experiment in terms of TOC removal
457 are summarized in Table 3.

458

459 **Tab. 3.** Contribution of the single processes to the simulated saline wastewater purification in terms
460 of TOC reduction.

| **Parameter** | **Influent Slop** | **Biological Output** | **MBR output** | **PCR output** |
|---|---|---|---|---|
| TOC [mg $L^{-1}$] | 224±13.2 | 137±14.9 | 69±10.1 | 12±5 |
| Removal | | 38.9% | 69.1% | 94.6% |

461 * average values ± standard deviation; overall removal efficiency

462

463 As previously discussed, the slop was characterized by a TOC content of approximately 225 mg $L^{-1}$.
464 The biological process contributed for approximately 40%, on average, to the overall slop
465 purification, suggesting that a significant amount of organic molecules passed through without any
466 degradation. Nevertheless, the membrane was able to retain a large amount of organic molecules
467 within the system, whose size exceeded the molecular weight cut-off of the same membrane. This
468 resulted in a further decrease of the effluent TOC approximately to 70 mg $L^{-1}$, leading to an
469 additional retention of approximately 30% of the organic content from the biological output. The
470 subsequent photocatalytic treatment further reduced the TOC content to approximately 10 mg $L^{-1}$.
471 The photocatalytic contribution may be misinterpreted if considered only in terms of TOC reduction
472 (25%). Indeed, it has to be considered that the fraction photocatalytically abated would need a very

473 long reaction time to be degraded by the only biological treatment. This would imply bigger
474 bioreactor volumes and additional membrane restoring operations with higher operating costs. It is
475 worth noticing that, based on the results above reported the membrane fouling could represent a
476 considerable drawback. Indeed, the harsh environmental conditions, favor the formation of small
477 particles able to occlude the internal pores of the membrane. Furthermore, longer HRT promote
478 EPS hydrolysis, thereby increasing the amount of SMP, which could negatively affect the
479 membrane-fouling tendency by promoting the pore-blocking mechanism. Therefore, the decrease of
480 the HRT in the MBR system, due to the presence of the subsequent photocatalytic process, could
481 result in a considerable economic advantage. On the other hand, the biological treatment affords
482 clear solutions for the photocatalytic system, thus optimizing its efficiency in terms of light
483 penetration and generation of highly oxidizing active oxygen species responsible for the
484 degradation of bio-recalcitrant compounds. Coupling of such systems showed an excellent
485 degrading capacity toward complex organic molecules, thus achieving carbon removal percentages
486 higher than 95%.
487 This result was particularly relevant if compared with previous literature. Indeed, in previous
488 studies, it was reported that physical-chemical processes, in particular coagulation-flocculation
489 treatments, enabled low TOC removal efficiencies, of approximately 50%, thus suggesting that
490 these processes could be used only as a pre-treatment before further advanced processes (Di Bella et
491 al., 2014). Among the biological systems, MBR and MB-MBR (moving bed membrane bioreactor)
492 systems enabled a maximum removal efficiency of 87%, in which the biological process removed
493 approximately 50% of TOC (Di Bella et al., 2015; Piazzese et al., 2018). However, the authors
494 observed that the performance of the biological system decreased in the long-term, highlighting the
495 possible instability of the process especially referring to the fluctuation in the influent slop
496 composition. The best results in terms of TOC removal efficiency of slop were obtained with
497 granular activated carbon (GAC) system, which enabled approximately 90% of TOC removal for a
498 GAC dosage of 20 mg $L^{-1}$ (Campo et al., 2017). However, other authors stress that the relatively

fast saturation of the GACs required frequent regeneration processes that increase the operating costs. In another study, the combination of air-stripping and photocatalysis has been studied for hydrocarbon removal from slop (Cazoir et al., 2012). By using these combined processes, the authors obtained an effluent with an overall hydrocarbon content (as TPH) < 15 ppm according to MARPOL legislation. However, the authors found that a lot of volatile organic carbons substances were purged from the aqueous phase, leading to an environmental problem.

The results achieved in this study demonstrated that the coupling of biological and photocatalysis processes enabled the best results among those reported in other studies carried out on a similar wastewater, while ensuring very stable performances and removal efficiencies. Compared with previous literature, the results reported in this study demonstrated that the combination of membrane bioreactors and photocatalysis is an effective approach for the treatment of saline wastewater polluted with recalcitrant organic compounds. The effluent obtained from the MBR system was clear and without suspended solids allowed to achieve very high performances in the photocatalysis process, thus enabling very high quality water with low residual TOC concentration.

## Conclusions

This study investigated the treatment of a simulated shipboard slop in a pilot plant consisting of a MBR and a PCR acting in series. The achieved results demonstrated that the coupling of a biological and a photocatalytic processes enabled very high organic pollution removal (95%), resulting in low TOC concentration in the effluent (TOC < 10 mg $L^{-1}$). More precisely, the MBR system enabled a TOC removal of approximately 80%, although a not negligible residual pollution was observed. The subsequent photocatalytic treatment, efficiently degrade the bio-recalcitrant fraction in the presence of the light activated persulfate ions, producing clear water with very low organic content (TOC = 10 mg $L^{-1}$). The harsh environmental conditions in the MBR caused a significant modification in the activated sludge physical properties, which, in turns, negatively affected the membrane fouling. The main fouling mechanisms were the "cake layer deposition" and

525 the "pore blocking". The superficial cake layer deposition ($R_{C,irr}$) was the highest fraction of the
526 total resistance to filtration (75%), whereas the irreversible fouling due to pore blocking ($R_{PB}$)
527 accounted for approximately 20% of the total resistance. Nevertheless, the original permeability of
528 the membrane was successfully recovered (98%) after chemical cleanings, thereby suggesting that
529 the irremovable fouling due to pore-blocking was low.
530 The achieved results demonstrated that the proposed solution represents a sustainable and efficient
531 solution for the purification of complex matrices with high salt content. The biological treatment
532 affords clear solutions to the photocatalytic system, thereby optimizing its efficiency in terms of
533 light penetration and generation of highly oxidizing active oxygen species responsible for the
534 degradation of bio-recalcitrant compounds.
535
536
537 **References**


538 Apha, 2005. Standard Methods for the Examination of Water & Wastewater, American Public
539 Health Association.

540 Augugliaro, V., Cavallero, L., Marci, G., Palmisano, L., Pramauro, E., 1994. Influence of
541 operational variables on the photodegradation kinetics of Monuron in aqueous titanium dioxide
542 dispersions. Stud. Surf. Sci. Catal. 82, 713–720. https://doi.org/10.1016/S0167-
543 2991(08)63467-9

544 Augugliaro, V., Loddo, V., Marci, G., Palmisano, L., LopezMunoz, M.J., 1997. Photocatalytic
545 oxidation of cyanides in aqueous titanium dioxide suspensions. J. Catal. 166, 272–283.
546 https://doi.org/10.1006/jcat.1997.1496

547 Bellardita, M., Nazer, H.A. El, Loddo, V., Parrino, F., Venezia, A.M., Palmisano, L., 2017.
548 Photoactivity under visible light of metal loaded TiO2 catalysts prepared by low frequency
549 ultrasound treatment. Catal. Today 284, 92–99. https://doi.org/10.1016/j.cattod.2016.11.026

550 Campo, R., Giustra, M.G., Marchis, M. De, Bella, G. Di, 2017. Characterization and Treatment
551 Proposals of Shipboard Slop Wastewater Contaminated by Hydrocarbons. Water 9, 581.
552 https://doi.org/10.3390/w9080581

553 Campo, R., Mitra, S., Di Bella, G., 2017. Analysis of extracellular polymeric substances and
554 membrane fouling of a MB-MBR treating shipboard slops. J. Environ. Eng. (United States)
555 143. https://doi.org/10.1061/(ASCE)EE.1943-7870.0001260

556 Capodici, M., Cosenza, A., Trapani, D. Di, Mannina, G., Torregrossa, M., 2017. Treatment of Oily
557 Wastewater with Membrane Bioreactor Systems. Water 9, 412.

https://doi.org/10.3390/w9060412

Cataldo, S., Iannì, A., Loddo, V., Mirenda, E., Palmisano, L., Parrino, F., Piazzese, D., 2016. Combination of advanced oxidation processes and active carbons adsorption for the treatment of simulated saline wastewater. Sep. Purif. Technol. 171, 101–111. https://doi.org/10.1016/j.seppur.2016.07.026

Cazoir, D., Fine, L., Ferronato, C., Chovelon, J., 2012. Hydrocarbon removal from bilgewater by a combination of air-stripping and photocatalysis. J. Hazard. Mater. 235–236, 159–168. https://doi.org/10.1016/j.jhazmat.2012.07.037

Corsino, S.F., Torregrossa, M., Viviani, G., 2017. The role of extracellular polymeric substances (EPS) on aerobic granules formation: Comparison between a case of synthetic wastewater supply and another of industrial wastewater. Desalin. Water Treat. 61. https://doi.org/10.5004/dwt.2016.11120

de Oliveira, T.S., Corsino, S.F., Di Trapani, D., Torregrossa, M., Viviani, G., 2018. Biological minimization of excess sludge in a membrane bioreactor: Effect of plant configuration on sludge production, nutrient removal efficiency and membrane fouling tendency. Bioresour. Technol. 259, 146–155. https://doi.org/10.1016/j.biortech.2018.03.035

Di Bella, G., Di Prima, N., Di Trapani, D., Freni, G., Giustra, M.G., Torregrossa, M., Viviani, G., 2015. Performance of membrane bioreactor (MBR) systems for the treatment of shipboard slops: Assessment of hydrocarbon biodegradation and biomass activity under salinity variation. J. Hazard. Mater. 300, 765–778. https://doi.org/10.1016/j.jhazmat.2015.08.021

Di Bella, G., Di Trapani, D., Judd, S., 2018. Fouling mechanism elucidation in membrane bioreactors by bespoke physical cleaning. Sep. Purif. Technol. 199, 124–133. https://doi.org/10.1016/j.seppur.2018.01.049

Di Bella, G., Giustra, M.G., Freni, G., 2014. Optimisation of coagulation / flocculation for pre-treatment of high strength and saline wastewater : Performance analysis with different coagulant doses. Chem. Eng. J. 254, 283–292. https://doi.org/10.1016/j.cej.2014.05.115

DuBois, M., Gilles, K. a., Hamilton, J.K., Rebers, P. a., Smith, F., 1956. Colorimetric method for determination of sugars and related substances. Anal. Chem. 28, 350–356. https://doi.org/10.1021/ac60111a017

Judd, S., Judd, C., 2006. The MBR book, The MBR Book. https://doi.org/10.1016/B978-1-85617-481-7.X5000-4

Khataee, A.R., Kasiri, M.B., 2010. Photocatalytic degradation of organic dyes in the presence of nanostructured titanium dioxide: Influence of the chemical structure of dyes. J. Mol. Catal. A Chem. https://doi.org/10.1016/j.molcata.2010.05.023

Le-Clech, P., Chen, V., Fane, T.A.G., 2006. Fouling in membrane bioreactors used in wastewater treatment. J. Memb. Sci. https://doi.org/10.1016/j.memsci.2006.08.019

Lin, H., Zhang, M., Wang, F., Meng, F., Liao, B.Q., Hong, H., Chen, J., Gao, W., 2014. A critical review of extracellular polymeric substances (EPSs) in membrane bioreactors: Characteristics, roles in membrane fouling and control strategies. J. Memb. Sci. https://doi.org/10.1016/j.memsci.2014.02.034

Lowry, O.H., Rosebrough, N.J., Farr, A.L., Randall, R.J., 1951. Protein measurement with the

599 Folin-Phenol Reagent. J. Biol. Cemistry 193, 265–275.

600 Mannina, G., Cosenza, A., Di Trapani, D., Capodici, M., Viviani, G., 2016. Membrane bioreactors
601 for treatment of saline wastewater contaminated by hydrocarbons (diesel fuel): An
602 experimental pilot plant case study. Chem. Eng. J. 291, 269–278.
603 https://doi.org/10.1016/j.cej.2016.01.107

604 Marpol 73/78, 2006. MARPOL 73/78 and Annex I: An Assessment of its Effectiveness. J. Int.
605 Wildl. Law Policy 9, 175–194. https://doi.org/10.1080/13880290600728195

606 McCallum, J.E.B., Madison, S.A., Alkan, S., Depinto, R.L., Rojas Wahl, R.U., 2000. Analytical
607 Studies on the Oxidative Degradation of the Reactive Textile Dye Uniblue A. Environ. Sci.
608 Technol. 34, 5157–5164. https://doi.org/10.1021/es0008665

609 Meng, F., Chae, S.R., Drews, A., Kraume, M., Shin, H.S., Yang, F., 2009. Recent advances in
610 membrane bioreactors (MBRs): Membrane fouling and membrane material. Water Res.
611 https://doi.org/10.1016/j.watres.2008.12.044

612 Miyoshi, T., Aizawa, T., Kimura, K., Watanabe, Y., 2011. Characteristics of proteins involved in
613 membrane fouling in membrane bioreactors (MBRs) treating municipal wastewater: The
614 application of metaproteomic analyses. Desalin. Water Treat. 34, 150–155.
615 https://doi.org/10/5004/dwt.2011.2894

616 Piazzese, D., Corsino, S.F., Torregrossa, M., Bongiorno, D., Indelicato, S., Viviani, G., 2018. Effect
617 of a co-substrate supply in a MBR treating shipboard slop: Analysis of hydrocarbon removal,
618 biomass activity and membrane fouling tendency. Biochem. Eng. J.
619 https://doi.org/10.1016/j.bej.2018.10.003

620 Rodriguez, S.M., Richter, C., G??lvez, J.B., Vincent, M., 1996. Photocatalytic degradation of
621 industrial residual waters. Sol. Energy 56, 401–410. https://doi.org/10.1016/0038-
622 092X(96)00023-0

623 Salerno, C., Vergine, P., Berardi, G., Pollice, A., 2017. Influence of air scouring on the performance
624 of a Self Forming Dynamic Membrane BioReactor (SFD MBR) for municipal wastewater
625 treatment. Bioresour. Technol. 223, 301–306. https://doi.org/10.1016/j.biortech.2016.10.054

626 Sheng, G.P., Yu, H.Q., Li, X.Y., 2008. Stability of sludge flocs under shear conditions. Biochem.
627 Eng. J. 38, 302–308. https://doi.org/10.1016/j.bej.2007.07.026

628 Šíma, J., Hasal, P., 2013. Photocatalytic Degradation of Textile Dyes in aTiO 2 /UV System. Chem.
629 Eng. Trans. 32, 79–84.

630 Viero, A.F., de Melo, T.M., Torres, A.P.R., Ferreira, N.R., Sant'Anna, G.L., Borges, C.P., Santiago,
631 V.M.J., 2008. The effects of long-term feeding of high organic loading in a submerged
632 membrane bioreactor treating oil refinery wastewater. J. Memb. Sci.
633 https://doi.org/10.1016/j.memsci.2008.03.038

634 Yang, S., Chen, Y., Lou, L.-P., Wu, X., 2005. Involvement of chloride anion in photocatalytic
635 process. J. Environ. Sci. (China) 17, 761–765.

636 Zhang, X., Bishop, P.L., 2003. Biodegradability of biofilm extracellular polymeric substances.
637 Chemosphere 50, 63–69. https://doi.org/10.1016/S0045-6535(02)00319-3

638
639

**Acknowledgments**

This work was funded by the National Operational Programme for Research and Competitiveness 2007–2013 - Project "STI-TAM– PON 02; the Italian Ministry of Education, University and Research and Ministry of Economic Development".

**Figure captions:**

**Fig. 1:** Schematic scheme of the MBR-PCR pilot plant installation: MBR (a) and PR (b).

**Fig. 2:** Trends of the total suspended solid concentration (TSS) and volatile suspended solid/total suspended solid (VSS/TSS) ratio during the experiments (a); amount and composition of the EPS (b).

**Fig. 3:** TOC concentration in the inlet, outlet and supernatant of the MBR system (a); biological, physical and overall TOC removal efficiencies throughout the experiment (b).

**Fig. 4:** Total $R_T$ (a), specific resistances (b), and percentage of each resistance fraction with respect to the total fouling resistance (c1-c4).

**Fig. 5:** TOC values against the cumulative energy impinging the photocatalytic suspension (in the absence of NaCl) in the pilot scale reactor under natural sunlight irradiation in the presence of air, 0.2 g $L^{-1}$ of P25 and P25son, at ambient temperature and pressure. Initial TOC concentration: 55 mg $L^{-1}$.

**Fig. 6:** TOC values versus the cumulative energy impinging the solution downstream the biological treatment in the pilot scale reactor under artificial UV light irradiation in the presence of air, 20 g $L^{-1}$ NaCl, 0.2 g $L^{-1}$ of P25, at ambient temperature and pressure ($87^{th}$ day). After the solid line $K_2S_2O_8$ (2 g $L^{-1}$) was present in the system. Initial TOC concentration: 54 mg $L^{-1}$.

**Table captions:**

**Tab.1:** TOC values of five real slop samples. Standard error: ±0.05 mg·$L^{-1}$

**Tab. 2:** Composition and average characteristics of the synthetic slop.

666 **Tab. 3.** Contribution of the single processes to the simulated saline wastewater purification in terms

667 of TOC reduction.